TELAC REPORT 93-4

DAMAGE TOLERANCE AND ARREST CHARACTERISTICS OF PRESSURIZED GRAPHITE/EPOXY TAPE CYLINDERS

NAG1-991

presented at ASTM Fifth Symposium on
Composite Materials: Fatigue and Fracture

Claudia U. Ranniger, Paul A. Lagace, and Michael J. Graves
Research Assistant, Associate Professor, Assistant Professor

TELAC

Technology Laboratory for Advanced Composites
Department of Aeronautics and Astronautics
Massachusetts Institute of Technology
77 Massachusetts Avenue
Cambridge, Massachusetts 02139

May, 1993

ABSTRACT

An investigation of the damage tolerance and damage arrest characteristics of internally-pressurized graphite/epoxy tape cylinders with axial notches was conducted. An existing failure prediction methodology, developed and verified for quasi-isotropic graphite/epoxy fabric cylinders, was investigated for applicability to general tape layups. In addition, the effect of external circumferential stiffening bands on the direction of fracture path propagation and possible damage arrest was examined. Quasi-isotropic $[90/0/\pm45]_s$ and structurally anisotropic $[\pm45/0]_s$ and $[\pm45/90]_s$ coupons and cylinders were constructed from AS4/3501-6 graphite/epoxy tape. Notched and unnotched coupons were tested in tension and the data correlated using the equation of Mar and Lin. Cylinders with through-thickness axial slits were pressurized to failure achieving a far-field two-to-one biaxial stress state. Experimental failure pressures of the $[90/0/\pm45]_s$ cylinders agreed with predicted values for all cases but the specimen with the smallest slit. However, the failure pressures of the structurally anisotropic cylinders, $[\pm45/0]_s$ and $[\pm45/90]_s$, were above the values predicted utilizing the predictive methodology in all cases. Possible factors neglected by the predictive methodology include structural coupling in the laminates and axial loading of the cylindrical specimens. Furthermore, applicability of the predictive methodology depends on the similarity of initial fracture modes in the coupon specimens and the cylinder specimens of the same laminate type. The existence of splitting which may be exacerbated by the axial loading in the cylinders, shows that this condition is not always met. The circumferential stiffeners were generally able to redirect fracture propagation from longitudinal to circumferential. A quantitative assessment for stiffener effectiveness in containing the fracture, based on cylinder radius, slit size, and bending stiffnesses of the laminates, is proposed.

Suggestions for further work in these areas to better understand the mechanisms at work and thus provide a better predictive methodology are offered.

KEYWORDS: Damage tolerance, damage propagation, damage arrest, graphite/epoxy, structural scaling, stiffening strips.

INTRODUCTION

The internally-pressurized thin-walled cylinder is a structural configuration of interest to engineers. Examples of structures of this general shape include airplane fuselages, rocket motor casings, fuel tanks, and oil pipelines. Each of these structures contains notches which are integral to its function. Fuselages contain cutouts for windows and doors; fuel tanks and oil pipelines contain similar notches for valves or pressure gages. Furthermore, through-damage can arise from a number of events. Failure of the cylinder due to internal pressure loading can often occur in these areas. It is important, therefore, that an accurate quantitative measure and understanding of the cylinder's damage tolerance and damage arrest characteristics be obtained and that failure criteria and predictive methodologies be developed.

Cylinder fracture prediction methodologies may be divided into two categories: those which directly characterize cylinder fracture, and those which extrapolate the cylinder fracture load from flat plate fracture data. While the former approach seems more straightforward conceptually, the latter is, in general, easier to implement. This is in part due to the fact that while the testing of tensile coupons is a largely routine, low-cost effort, the testing of full-size cylindrical structures is not. By using coupons to predict cylinder failure, much of the preliminary cylinder testing can be replaced with simple coupon tests and analysis.

Such a methodology to predict the fracture pressure of notched internally-pressurized composite cylinders has been proposed [1,2]. The prediction uses notched coupon fracture data and material properties to determine the fracture pressure of cylindrical specimens by accounting for the increased stress intensities of the notch due to the effects introduced by the internally-pressurized shell configuration. However, this methodology was developed and has been verified only

for the case of quasi-isotropic fabric cylinders [1-5]. It is important to examine the extent to which this methodology is applicable to composite cylinders of general configuration.

The fracture of notched pressurized cylinders of general laminate configurations and the limits of using tensile coupon data to predict these failure pressures are thus investigated. In the current investigation, the applicability of such a fracture prediction methodology to quasi-isotropic $[90/0/\pm45]_s$ and structurally anisotropic $[\pm45/0]_s$ and $[\pm45/90]_s$ AS4/3501-6 graphite/epoxy tape cylinders is examined by experimentally finding the fracture pressures and modes of such specimens. In addition, studies of the fracture paths and fracture data are used to examine the mechanisms of failure.

In addition to the ability of a structure to not fracture in the presence of damage (damage tolerance), it is also important to be able to arrest damage which propagates. Damage arrest in composite materials has been studied both in plate and shell structures [1,2,6,7,8,9]. In the case of internally-pressurized cylinders, it has been demonstrated that damage can be turned (though not yet completely arrested) through the use of unidirectional circumferential stiffening bands [1,2]. It has been proposed that the fracture will propagate in the direction perpendicular to the orientation of the maximum tensile strain and this has been demonstrated in quasi-isotropic graphite/epoxy fabric layups [9]. However, it is not known how the coupling of bending-twist deformation in a structurally anisotropic layup or the use of a graphite/epoxy tape will affect this fracture propagation, redirection and potential arrest in the composite cylinder. The second purpose of this investigation is, thus, to determine the effects of circumferential stiffening bands on the failure propagation of structurally anisotropic cylinders with notches and to further identify the parameters governing fracture path redirection.

The current experimental work includes both coupon and cylinder tests. The notch sensitivity of tensile coupons with slits is determined experimentally, and the

results are used to predict the fracture of cylinders with through-the-thickness axial slits. Axially-slit cylinders are subsequently pressurized to failure, and the results compared with the predicted fracture pressures. Different stiffener configurations are laid up on the outer surface of the cylinders, and fracture paths are examined after failure. Qualitative as well as quantitative evaluations of the failure path and of the ability of the stiffeners to alter the direction of damage propagation are made.

PREDICTIVE/CORRELATIVE METHODOLOGY

The basic methodology proposed by Graves and Lagace [1] has several key parts: the correlation for notched coupon fracture, assumptions concerning the applicability of coupon data to the pressurized cylinder, and analysis to account for the geometrical effects of the shell.

The flat-plate fracture correlation developed by Mar and Lin [10, 11] is utilized to characterize the notched tensile fracture of uniaxially loaded coupons. The far-field fracture stress of a notched composite plate under uniaxial tension is correlated via:

$$\sigma_f = H_c\,(2a)^{-m} \tag{1}$$

where 2a is the length of the notch transverse to the loading direction, H_c is defined as the laminate fracture parameter [12], and m is the value of the stress singularity at a notch tip at the fiber-matrix interface. The composite fracture parameter, H_c, is determined experimentally and is a function of layup. The exponent m, which has been determined analytically to be 0.28 for graphite/epoxy, is a function of the shear moduli and Poisson's ratios of the fiber and matrix [13]. Experimental work has indicated that the correlation is applicable to both tape and fabric graphite/epoxy laminates containing holes or slits oriented arbitrarily relative to the loading axes

[3,12,14] and that while H_c is dependent on the laminate, it is not dependent on the notch geometry.

In developing predictive methodology for cylinder failure, it is important to consider factors associated with the fact that the stress state of a pressurized cylinder with an axial notch is different from that of flat plates. Internal pressure induces both biaxial loading (a 2:1 radial to axial state of stress) and bulging of the cylinder at the precut slit. The resulting extensional and bending stresses at the slit ends and edges, as well as the bending-extensional stress coupling introduced by the curved shell geometry, can contribute to cylinder fracture. Thus, in order to utilize the coupon data for the cylinder case, two important assumptions are made. The first is that the axial stress does not contribute to failure. It has been shown that the tensile fracture stress of uniaxially-loaded coupons is not reduced by a notch oriented along the direction of load [15]. Thus, only the hoop stress is considered as a primary cause of failure in the pressurized cylinder with axial notches. The second assumption is that the same failure mechanisms occur in the cylinder as in the coupons. This, of course, cannot be verified until after tests have been conducted. If this latter assumption is not met, then the laminate fracture parameter used to characterize the notched fracture response will not be representative of the behavior of the cylinder since different fracture mechanisms would be operative.

A second factor to consider is that the shell curvature causes an intensification of the local membrane stresses due to the bulging effects. Folias [16,17,18] used eighth order shell theory to determine this effect on the stress field at slit ends in isotropic shells. He proposed stress intensity factors, depending on shell geometry, slit size, material properties, and applied loading, to account for the increase in local stresses at the slit tip in a pressurized shell over those found for a similarly-notched plate. For an axial slit in a cylindrical shell loaded via internal pressure, the

extensional stress intensification factor, representing the increase in local extensional stresses at the slit tip in a shell, can be approximated as

$$K_i = (1 + 0.317\lambda_i^2)^{0.5} \tag{2}$$

where the isotropic shell parameter λ_i^2 is a function of laminate properties and specimen geometry:

$$\lambda_i^2 = a^2[12(1-\nu^2)]^{0.5}/rt \tag{3}$$

and where t is the cylinder thickness, r is the cylinder radius, a is the half-slit length, and ν is the Poisson's ratio of the laminate.

Given these basic parts of the methodology, the fracture stress relation between an axially-slit cylinder and a notched coupon can be rewritten as a function of far-field stresses and the stress intensity factor of equation (2) as:

$$\sigma_{cyl} = \sigma_f / K_i \tag{4}$$

where σ_{cyl} is the far-field circumferential stress of a cylinder at fracture, σ_f is the far-field fracture stress in a plate under uniaxial tension, and K_i is the extensional stress intensification factor. The far-field circumferential stress of the cylinder is related to the pressure via:

$$\sigma_{cyl} = pr/t \tag{5}$$

The cylinder failure pressure can thus be determined by setting the far-field circumferential stress of equation (5) equal to the cylinder critical value in equation (4) as determined by the coupon correlation of equation (1). This results in:

$$p_f = H_c t / [K_i r (2a)^{-m}] \quad (6)$$

which is the final expression for the internal pressure of a cylinder at failure.

EXPERIMENTAL PROCEDURE

All the experimental work, with one exception, in this investigation was done with specimens manufactured from Hercules AS4/3501-6 graphite/epoxy tape with a nominal thickness of 0.134 mm. A quasi-isotropic $[90/0/\pm45]_s$[1] tape laminate was chosen in order to compare results with previous work conducted on quasi-isotropic $[0_f/45_f]_s$[2] fabric cylinders. Structurally anisotropic layups of $[\pm45/90]_s$ and $[\pm45/0]_s$ were chosen for several reasons. These are layups which are relatively easy to manufacture and for which coupon fracture data already exists [12]. The two layups are complementary in that the $[\pm45/0]_s$ has fibers in the direction of circumferential stress and the $[\pm45/90]_s$ has fibers along the axial loading and slit axes. Thus, the effects of having fibers along either of the two directions of principal loading can be examined. The use of these two layups also helps to determine which failure characteristics are laminate-specific and which are due to the structural anisotropy of the laminates. Both coupon and cylinder specimens were manufactured and tested for all three laminate configurations. Full details are given in Reference [19].

Coupons

Uniaxial tensile tests were conducted on coupons of the geometry shown in Figure 1 in both notched and unnotched configurations in order to obtain values for the

---

[1] For the cylinder, the 0° direction is along the circumference.
[2] The subscript "f" indicates fabric.

composite fracture parameter, H_c. Although notch geometry has been shown to have little effect on coupon fracture stresses, slits perpendicular to the applied uniaxial load were chosen as the notch types so that fracture of the coupons and cylinders could be directly compared. Slit sizes of 9.5, 12.7, 15.9, and 19.1 mm were used, and a coupon width of 70 mm was chosen to avoid finite width influences on coupon failure. Four specimens of each slit size (eight for the unnotched case) and each laminate configuration were manufactured.

Six 350 by 305 mm laminates were manufactured from AS4/3501-6 material for each layup. The laminates were processed as 350 mm by 305 mm plates using the standard manufacturer's cure cycle of a one-hour flow stage at 116°C and a two-hour set stage at 177°C. This was conducted in an autoclave under vacuum with a 0.59 MPa external pressure. These laminates were then postcured in an oven at 177°C for eight hours and subsequently cut into four coupons 70 mm wide using a water-cooled diamond wheel. Glass/epoxy loading tabs with a 0/90 configuration were bonded to the ends of all coupons with American Cyanamid FM-123 film adhesive. Slits were cut in some specimens, as previously indicated, with a diamond grit end mill 0.74 mm in diameter mounted on a rotary tool with a speed of 30,000 rpm. Slit ends were notched with a hand-held jeweler's saw. A far-field strain gage was placed on each coupon to verify specimen quality via modulus measurement.

Uniaxial tensile tests were conducted monotonically to failure on an MTS 810 testing machine under stroke control at a rate of 1.1 mm/min. This yields a strain rate of approximately 5000 microstrain/minute in the test section. Stroke, load, and strain data were recorded automatically at a rate of 2 Hz until coupon failure occurred.

Cylinders

Cylinders of the configuration shown in Figure 2 were manufactured and tested. These cylinders were of the same layup as the coupons. A cylinder radius of 152 mm

was chosen to match the experimental work done in previous investigations and a cylinder length of 760 mm was selected to assure that initial failure at the slit and damage arrest by the stiffeners did not interfere with one another. Slit lengths ranged from 12.7 to 63.5 mm as shown in the test matrix of Table 1.

Cylinders were laid up on a cylindrical mandrel and cured using the same cure and postcure cycles as for the coupons. The stiffeners were made of unidirectional tape 76 mm in width and were laid up on the external surface of the $[\pm 45/90]_s$ and $[\pm 45/0]_s$ cylinders prior to cure. The stiffeners were placed 305 mm apart center to center as shown in Figure 2. The number of stiffeners was chosen so that the effect of a range of bending stiffnesses could be examined. The number of stiffener layers varied from zero to four, as indicated in Table 1, increasing the bending stiffness of the region, in the circumferential direction, up to 20 times that of the base laminate. It should be noted that two individual tests, determination of both fracture initiation load and fracture propagation characteristics, are being conducted with each cylinder specimen.

Due to unexpectedly high failure pressures obtained for the structurally anisotropic cylinders with 12.7 mm long slits, a $[0_f/45_f]_s$ quasi-isotropic fabric cylinder with the same slit size was manufactured and tested for comparison between tape and fabric configurations. The same procedures were utilized. The fabric was a five-harness satin weave version of the AS4 fibers in 3501-6 epoxy: Hercules AW370-5H/3501-6S.

Slits in all the cylinders were cut with a 30,000 rpm rotary tool with a 25 mm diameter composite blade mounted vertically on a milling machine arm. Slits were cut to the correct length and notched at the tips by hand with a small jeweler's saw. An even and smooth area away from the ply seams was chosen for the location of the slit. Due to the destructive nature of the tests, a 50 mm by 50 mm grid was drawn on the

entire exterior surface of each cylinder with white paint. The grid squares were individually labelled to facilitate post-test reassembly of the remaining fragments.

Cylinder testing was accomplished via pressurization using bottled nitrogen. This required sealing of the cylinders. The cylinders were sealed at both ends by bonding them in grooves cut into aluminum endcaps. Internal rubber bladders, made of 0.8 mm thick gum rubber, were placed inside each cylinder to contain the pressurizing gas. The cylinders were attached to pressure transducers so that internal pressure at failure could be recorded.

Cylinder testing was conducted in a blast chamber. A cylinder was placed horizontally on an iron channel in the center of the blast chamber. The cylinder, which rested on its endcaps, was oriented "slit up" so that the majority of the failure path would not be constrained by the channel. The ends of the cylinder were not fixed to the channel, and no restrictions were made on axial movement or expansion of the cylinder. Cylinder pressurization was controlled manually with the use of a pressure regulator attached directly to a nitrogen tank at an approximate rate of 0.4 MPa/minute. The pressurization rate was monitored during the test via a dial gage and a chart recording of the pressure transducer output. Data, including internal cylinder pressure, was collected at 0.5 second intervals.

Photographs were taken of all coupons and cylinders after testing to record failure modes. Drawings of fracture patterns were made for each coupon type and for all cylinders. These were used to identify the primary fracture path as well as determine stiffening band effects on the failure. Data reduction to stresses utilized the nominal tape ply thickness of 0.134 mm (0.35 mm for the one fabric cylinder) which was acceptably close to the average measured per ply thickness of 0.140 mm for the coupons and 0.141 mm for the cylinders.

DAMAGE TOLERANCE

Experimental results are presented herein along with predictions and correlations. Application of the predictive methodology to the structurally anisotropic tape cylinders was not expected to yield accurate results, but is made to assess the quantitative difference which results from the anisotropy of the laminate.

Coupon Results

Nominal slit sizes, coupon widths, and laminate thicknesses were used to calculate the fracture parameter H_c from the notched specimens using the Mar-Lin correlation. The average H_c value is 664 MPa(mm)$^{0.28}$ with a coefficient of variation of 4.2% for the $[90/0/\pm45]_s$ notched coupons, 715 MPa(mm)$^{0.28}$ with a coefficient of variation of 5.6% for the $[\pm45/0]_s$ coupons, and 422 MPa(mm)$^{0.28}$ with a coefficient of variation of 4.3% for the $[\pm45/90]_s$ coupons. The stress correlations and the notched coupon data are shown in Figures 3, 4, and 5.

The coupons of each laminate configuration showed the same fracture characteristics independent of slit size. Typical photographs are shown in Figure 6. In all cases, fracture originated at the slit ends and propagated outward. In the $[90/0/\pm45]_s$ coupons, the fracture travelled along the ±45° directions approximately halfway to the coupon edge from the slit ends before turning to 90° and running parallel to the slit. The 0° fibers, aligned with the tensile load, broke cleanly along this fracture path. The fibers oriented at 90° did the same, but secondary delamination from the surface of the coupon was observed. The fracture path in the $[\pm45/0]_s$ coupons is typically oriented at a -45° angle, perpendicular to the direction of the surface fibers, from the slit tip to the edge of the laminate. Secondary delamination of the external 45° plies along the fracture path results in a 'butterfly' fracture pattern

extending from both ends of the slit to the edges of the laminate. No delamination of internal plies is visible.

In the $[\pm 45/90]_s$ notched specimens, the fracture path lies along the -45° direction with the internal -45° and 90° plies fracturing cleanly along this line. The external +45° fibers exhibit matrix cracking and delamination from underlying plies in the region around the primary fracture.

Cylinder Results

Failure pressure prediction for the quasi-isotropic $[90/0/\pm 45]_s$ cylinders was determined with the appropriate coupon data. A graph of failure pressure versus slit size is presented in Figure 7. The graph includes the Mar-Lin correlation curve determined from the $[90/0/\pm 45]_s$ coupons as well as the corrected shell prediction for the quasi-isotropic cylinders. Comparison of the experimental cylinder failure pressures and the predicted curve indicates that, for the larger slit sizes, the predictive methodology is accurate. However, the experimentally-determined failure pressure of the cylinder with the 12.7 mm slit is not only much higher than the predicted value, but is also greater than the coupon correlation found for the same slit size.

Failure pressures for the structurally anisotropic cylinders were estimated from the coupon data as described previously. As previously indicated, since the properties of the structurally anisotropic cylinders cannot adequately be described by the predictive methods used here, the predicted failure pressures cannot be expected to match the experimental results. The predictive methodology is presented both as an estimate of the range of failure pressures and because the difference between the predicted and experimental results is indicative of the applicability, or lack thereof, of the predictive method.

These experimental and predicted failure pressures for the $[\pm 45/0]_s$ and $[\pm 45/90]_s$ cylinders are presented in Figures 8 and 9. In both series, the experimental

data for the cylinders with larger slit sizes falls between the plate and shell prediction curves. For smaller slits, the failure pressures are near the plate values. As the slit size increases the failure pressures are closer to the shell prediction curves. The failure pressure of the specimens with the 12.7 mm slit, however, are not only well above the shell predictions, but are higher than the equivalent plate data as well.

The failure pressure of the $[0_f/45_f]_s$ quasi-isotropic fabric cylinder with the 12.7 mm long slit is plotted with a plate correlation and quasi-isotropic shell failure prediction in Figure 10. The plate data, acquired in previous work, was found for the same material and layup [20] with a value of H_c of 750 MPa(mm)$^{0.28}$. Cylinder data, determined in previous work for larger slit sizes [9], is also included to provide a basis for comparison of the data and predicted results. Unlike the data for the graphite/epoxy tape cylinders with 12.7 mm slits, the failure pressure of the fabric cylinder agrees well with the predicted value.

This comparison of experimental cylinder data with predicted fracture pressures shows that the methodology applied in this investigation does not adequately predict the fracture pressures of structurally anisotropic cylinders. Furthermore, the fracture pressures of both the quasi-isotropic and structurally anisotropic graphite/epoxy tape cylinders with 12.7 mm slits are greater than the equivalent stresses for coupons with the same slit sizes.

An overriding assumption of the predictive methodology applied in this investigation is that the initial fracture modes of the cylinders are similar to those for the coupons of the same laminate. It is therefore necessary to carefully examine and compare the fracture modes of the coupons and cylinders, particularly the initial fracture which is not influenced by the effects of finite width and stiffener placement. Comparison of coupon and cylinder fracture modes indicates that the initial fracture modes are not always similar.

The initial fracture paths in the $[90/0/\pm45]_s$ cylinders are similar to those found in the tensile coupons except in the case of the cylinder with the 12.7 mm slit. This can be seen in the photograph of Figure 11 for the case of a cylinder with a 50.8 mm slit where the fracture path originally runs off at a 45° angle to the slit and load. However, the cylinder with the 12.7 mm slit does have a different fracture scenario as is shown in Figure 12 where, in addition to two paths which extend at 90° and proceed directly to the endcaps, another extends in the 0° (circumferential) direction from the slit end. In the case of larger slit sizes, the fracture path often turns in the circumferential direction away from the original slit. In the case of the cylinder with the 12.7 mm slit, the circumferential fracture extends directly from the slit end, and continues for 80 mm before splitting to form two axial fracture paths which contribute greatly to the overall damage in the cylinder. This indicates that a different initial fracture mode may dominate in this latter cylinder and would explain why the predictive methodology fails at this point. However, only one specimen of this configuration was tested and the test should be repeated to acquire better assurance. Furthermore, the failure pressure of the quasi-isotropic fabric cylinder with a 12.7 mm slit is accurately predicted by the current methodology. Thus, further investigation of the differences in fracture modes of tape and fabric cylinders particularly at small slit sizes is called for.

For both anisotropic laminate configurations, there are differences in the fracture modes between the coupons and cylinders. In the $[\pm45/0]_s$ cylinders, the original fracture is quite different from the coupon specimens as four fracture paths originate at the slit ends and extend primarily in the 0° and ±45° directions. This is shown for a representative case in Figure 13. The $[\pm45/0]_s$ notched coupons showed two fracture paths oriented at -45° at the slit ends.

In the $[\pm45/90]_s$ cylinders and notched coupons, two fracture paths originate at the slit ends. However, in the coupons these fracture paths are oriented at -45° angles while they extend in the 90° direction from the slit ends before bifurcating to ±45°

between 20 and 200 mm from the slit in the cylinders, as is shown in the representative photograph presented in Figure 14. The appearance of the fracture surface is similar to that seen in the tensile coupons although the angle of fracture propagation does differ.

Since there are significant differences in the initial fracture paths of the structurally anisotropic coupons and cylinders, and of the $[90/0/\pm45]_s$ coupons and the cylinder with the 12.7 mm slit, application of the predictive methodology to these specimens is not expected to be valid. The key question is what effects cause these fracture modes to differ and therefore what effects need to be included in the predictive methodology. Two possible effects which should be considered are suggested.

One possible effect is that the bending-twisting coupling inherent in the anisotropic laminates will change the stress state at the slit in the cylinders, due to the local bending. This does not affect the tensile coupons due to the lack of bending.

The second possible effect involves the broadest assumption made in applying the current predictive methodology in that the axial loading of the cylinder does not affect the fracture stress. This assumption may be less valid in the case of anisotropic laminates than for the case of quasi-isotropic laminates, particularly when tape material is utilized. Whereas splitting cannot occur in fabric, it can occur in tape and may allow axial load to play a more important role. Previous work [21,22,23] on tape laminates in uniaxial tension indicates that splitting in 0° plies accompanied by delamination are quite effective in mitigating stress in tape laminates and can thereby reduce notch sensitivity. Examination of the $[90/0/\pm45]_s$ cylinder with the 12.7 mm slit shows that a circumferential fracture originates at the slit end. This fracture may indicate the development of a split in the 0° ply which reduced the local stress state, resulting in a higher specimen failure pressure. This stress mitigation does not occur in the quasi-isotropic fabric cylinder with the same slit size as axial splitting is limited by the woven nature of the fabric.

DAMAGE ARREST

In none of the cases was the fracture totally arrested. However, in all the cylinder specimens, the fracture path generally bifurcates into two fracture paths as it moves away from the original slit. This can be seen in Figure 15. In most cases, as the fracture nears a stiffener or endcap, the fracture path will be further redirected. This effect was classified into three categories: through, into, and turned. These words correspond to the extent of the fracture path relative to the stiffener location. "Through" indicates that at least one fracture path has extended entirely through the stiffening band (this is always the classification for an unstiffened cylinder). "Into" indicates that a fracture path has travelled at least partway into the stiffened region. "Turned" indicates that the fracture path has been turned to 0° (circumferential) at the inside edge of the stiffener or within the stiffener. More than one term may apply to any one cylinder.

The classification of the $[\pm 45/0]_s$ and $[\pm 45/90]_s$ cylinders are contained in Tables 2 and 3. In addition, a "containment ratio" is shown for each specimen. This ratio is an attempt to quantify the likelihood that damage will be contained in a particular configuration. Such a ratio must include factors such as the energy of the system as well as the geometrical factors which can affect containment.

In all cases, the fractures of the specimens with the smallest slit sizes are most severe. As slit size decreases, more force in the form of internal pressure is required to produce the same local stresses. The slit size can therefore be used as an inverse measure of the energy which must be dissipated in the fracture and pressure release processes. More energy, provided by the internal pressure, is available to promote fracture propagation in the cylinders with small slits; consequently, more damage occurs. Since the pressure is related to the size of the slit and the inverse of the

cylinder ratio (see equation (6)), the nondimensional ratio 2a/r is used to characterize the energy provided by the internal pressure.

Circumferential stiffening bands are thought to affect the direction of fracture propagation by lowering circumferential strains in the laminate [9]. Thicker layers of stiffeners, which are more resistant to the bending which occurs as the damage propagates, thus further lower the local circumferential strains. The ratio of bending stiffnesses of the stiffened (D_s) to unstiffened regions (D_u) of the cylinder can therefore be used as a measure of the effectiveness of a stiffener in containing fracture.

The laminate-specific containment ratio, C, dependent upon these two measures is therefore:

$$C = (D_s/D_u)\ (2a/r) \tag{7}$$

The value of the containment ratio increases with the likelihood of turning or containing damage originating at a slit end between the set of stiffeners. As the radius of a cylinder approaches infinity and the specimen approximates a flat plate, the value of the containment ratio approaches zero. Previous work [6] shows that similar stiffeners have no effect on the direction of notch propagation in flat plates. This supports the use of the radius, r, in the denominator of the containment ratio.

The qualitative and quantitative measures of cylinder damage correlate within each laminate type, with the exception of the $[\pm 45/0]_s$ cylinder with two stiffeners and a 63.5 mm slit, as a minimum containment ratio exists above which the damage is turned. This value is between 1.50 and 2.09 for the $[\pm 45/0]_s$ cylinders and is in the vicinity of 2.0 for the $[\pm 45/90]_s$ cylinders. It is important to note that the correlations are laminate specific. The applicability of this containment ratio to other cylinder types is thus untested. It is not known what effect variation of the specimen geometry will have on the applicability of the containment ratio to categorize fracture. It is suggested that

tests on cylinders of various radii and with various slit sizes be conducted to determine the applicability of this containment ratio.

SUMMARY

The fracture of notched pressurized cylinders of general (quasi-isotropic and structurally anisotropic) tape laminate configurations and the limits of using tensile coupon data to predict these failure pressures was investigated. The fracture prediction methodology was previously shown to be valid for quasi-isotropic cylinders made from graphite/epoxy fabric.

This predictive methodology was able to predict the failure pressure of the $[90/0/\pm45]_s$ quasi-isotropic tape cylinders with axial slits ranging from 25.4 to 63.5 mm in length, but was unable to predict the failure pressure of the $[90/0/\pm45]_s$ cylinder with the 12.7 mm long slit. For all cases in the structurally anisotropic cylinders, $[\pm45/0]_s$ and $[\pm45/90]_s$, the predictive methodology was unable to predict the failure pressure. Stress mitigation at the notch tip, caused by axial splitting of the 0° ply and local delamination in the region near the slit, may explain the inability of the predictive methodology to determine the failure pressures in these cases. This may also allow the axial stress to play an important role. In all these cases, the fracture modes observed in the cylinders were different than those observed in the coupons of the same laminate. In the cases where the predictive methodology is accurate, these failure modes are the same. In addition, stress coupling, specifically bending-twisting, inherent in these structurally anisotropic laminates may contribute to a changed stress intensification at the notch tip which results in a difference in the failure pressure.

Both quasi-isotropic and structurally anisotropic tape cylinders with small slits should be examined to better understand the role of the tape splitting in the failure process. Sub-failure pressurization of cylinders and subsequent evaluation of the

damage in the region around the slit should be done. In addition, experiments should be done on pressurized cylinders where the axial stress is not carried by the cylinder in order to assess the role of the axial stress in the failure of these cases.

In addition to the work on damage tolerance, damage arrest characteristics of these configurations were also determined. External stiffeners located on either side of the slits were generally able to redirect fracture paths from the axial to the circumferential direction. The ability of the stiffening bands to contain damage depends both on the slit size and the number of stiffener layers present in the cylinder. Quantification of this effect via a suggested parameter known as the containment ratio successfully ranked the structurally anisotropic cylinders according to the amount of damage extending through the stiffeners. This containment ratio depends on slit length, cylinder radius, and the bending stiffnesses of the stiffened and unstiffened regions. The effects of alterations of cylinder radius, slit size, and stiffener layup on the containment ratio should be further evaluated experimentally to determine the relative importance of these factors in damage arrest and its quantification. In addition, comparison of containment ratios for different laminate types should be conducted to assess the generality of the containment ratio.

In addition to the specific implications of this data, this work continues to indicate a more general methodology by which data obtained from laboratory scale coupons can be utilized to predict the behavior of particular structural configurations by accounting for the particular stress intensification factors which the geometry introduces. This methodology is based on the assumption that the fracture behavior observed in the coupon specimens is the same as that manifested at the structural level. Otherwise, fracture data which characterizes the coupon behavior will not be representative of the structural behavior.

ACKNOWLEDGEMENTS

This work was sponsored by the NASA Langley Research Center under NASA Grant NAG-1-991.

REFERENCES

1. Graves, M.J., and Lagace, P.A., "Damage Tolerance of Composite Cylinders," *Composite Structures*, Vol. 4, No. 1, 1985, pp. 75-91.

2. Graves, M.J., "The Catastrophic Failure of Pressurized Graphite/Epoxy Cylinders," TELAC Report 82-10, Massachusetts Institute of Technology, Cambridge, MA, September 1982.

3. Chang, S.G. and Mar, J.W., "The Catastrophic Failure of Pressurized Graphite/Epoxy Cylinders Initiated by Slits at Various Angles," *Journal of Aircraft*, Vol. 22, No. 6, June 1985, pp. 462-466.

4. Lagace, P.A. and Saeger, K.J., "Damage Tolerance Characteristics of Pressurized Graphite/Epoxy Cylinders," *Proceedings of the Sixth International Symposium on Offshore Mechanics and Arctic Engineering*, ASME, Houston, Texas, March,1987, pp. 31-37.

5. Saeger, K.J., and Lagace, P.A., "Fracture of Pressurized Composite Cylinders with a High Strain-to-Failure Matrix System," *Composite Materials: Fatigue and Fracture, Second Volume, ASTM STP 1012*, ASTM, 1989, pp. 326-337.

6. Sawicki, A.J., Graves, M.J., and Lagace, P.A., "Failure of Graphite/Epoxy Panels with Stiffening Strips", *Composite Materials: Fatigue and Fracture, Fourth Volume, ASTM STP 1156*, ASTM, 1993, pp. 5-34.

7. Bhatia, N.M., and Verette, R.M., "Crack Arrest of Laminated Composites," *Fracture Mechanics of Composites, ASTM STP 593*, ASTM, 1975, pp. 200-214.

8. Jozavi, H., Dupuis, C.W., and Sancaktar, E., "An Investigation of the Fracture Behavior of a Composite Crack Arrestor," *Journal of Composite Materials*, Vol. 22, No.5, May, 1988, pp. 427-446.

9. Graves, M.J., and Sawicki, S.M., "The Failure of Integrally Stiffened Graphite/Epoxy Cylinders", submitted to *Composite Structures*.

10. Mar, J.W., and Lin, K.Y., "Fracture of Boron/Aluminum Composites with Discontinuities," *Journal of Composite Materials*, October, 1977, pp. 405-421.

11. Mar, J.W., and Lin, K.Y., "Fracture Mechanics Correlation for Tensile Failure of Filamentary Composites with Holes," *Journal of Aircraft*, Vol. 14, July, 1977, pp. 703-704.

12. Lagace, P.A., "Notch Sensitivity and Stacking Sequence of Laminated Composites," *Composite Materials Testing and Design, ASTM STP 893*, ASTM, 1986, pp. 161-176.

13. Fenner, D.N., "Stress Singularities in Composite Materials with an Arbitrarily Oriented Crack Meeting an Interface," *International Journal of Fracture*, Vol. 12, No. 5, October, 1986, pp. 705-721.

14. Lagace, P.A., "Notch Sensitivity of Graphite/Epoxy Fabric Laminates," *Composites Science and Technology*, Vol. 26, 1986, pp. 95-117.

15. Brewer, J.C., "Tensile Fracture of Graphite/Epoxy with Angled Slits," TELAC Report 82-16, Massachusetts Institute of Technology, December, 1982.

16. Folias, E.S., "On the Effect of Initial Curvature on Cracked Flat Sheets," *International Journal of Fracture Mechanics*, Vol. 5, No. 4, 1969, pp. 327-346.

17. Folias, E.S., "An Axial Crack in a Pressurized Cylindrical Shell," *International Journal of Fracture Mechanics*, Vol.1, No.2, 1965, pp. 104-113.

18. Folias, E.S., "On the Prediction of Catastrophic Failures in Pressurized Vessels," *Prospects of Fracture Mechanics*, edited by G.C. Sih, H.C. van Elst, and D. Broek, Nordhoff International, Leiden, the Netherlands, 1974, pp. 405-418.

19. Ranniger, C., "Damage Tolerance and Arrest Characteristics of Pressurized Graphite/Epoxy Tape Cylinders," TELAC Report 91-11, Massachusetts Institute of Technology, Cambridge, MA, June, 1991.

20. Ranniger, C., "Effect of Cylinder Diameter on the Damage Tolerance of Graphite/Epoxy Cylinders with Axial Notches," TELAC Report 91-10, Massachusetts Institute of Technology, Cambridge, MA, May, 1991.

21. Lagace, P.A., Bhat, N.V., and Gundogdu, A., "Response of Notched Graphite/Epoxy and Graphite/PEEK Systems", *Composite Materials: Fatigue and Fracture, Fourth Volume, ASTM STP 1156*, ASTM, 1993, pp. 55-71.

22. Harris, C.E., and Morris, D.H., "A Fractographic Investigation of the Influence of Stacking Sequence on the Strength of Notched Laminated Composites," *Fractography of Modern Engineering Materials: Composites and Metals, ASTM STP 948*, ASTM, 1987, pp. 154-173.

23. Lagace, P.A., and Nolet, S.C., "The Effect of Ply Thickness on Longitudinal Splitting and Delamination in Graphite/Epoxy under Compressive Cyclic Load",

Composite Materials: Fatigue and Fracture, ASTM STP 907, ASTM, 1986, pp. 335-360.

Table 1 Test Matrix for Cylindrical Specimens

Slit length [mm]	Laminate[a]			
	$[90/0/\pm45]_s$	$[\pm45/0]_s$	$[\pm45/90]_s$	$[0_f/45_f]_s$[b]
12.7	0[c]	4	4	0
25.4	0	0	0	-
38.1	0	4	0	-
50.8	0	2	4	-
63.5	-	2	2	-

[a] One specimen tested for each entry (except no specimen for entry of "-").

[b] Subscript "f" indicates fabric.

[c] Indicates number of stiffener plies on cylinder.

Table 2 Fracture Propagation/Arrest Assessment of $[\pm 45/0]_s$ Cylinders

Slit Size [mm]	Number of Stiffener Layers	Containment Ratio	Qualitative Fracture Description
12.7	4	1.50	through
25.4	0	0.17	through
38.1	4	4.49	turned
50.8	2	2.09	into/turned
63.5	2	2.61	through/turned[a]

[a] Fracture extends through the stiffeners but turns before reaching the endcaps.

Table 3 Fracture Propagation/Arrest Assessment of $[\pm 45/90]_s$ Cylinders

Slit Size [mm]	Number of Stiffener Layers	Containment Ratio	Qualitative Fracture Description
12.7	4	1.65	through/turned
25.4	0	0.17	through
38.1	0	0.25	turned
50.8	4	6.62	into/turned
63.5	2	2.85	through/turned

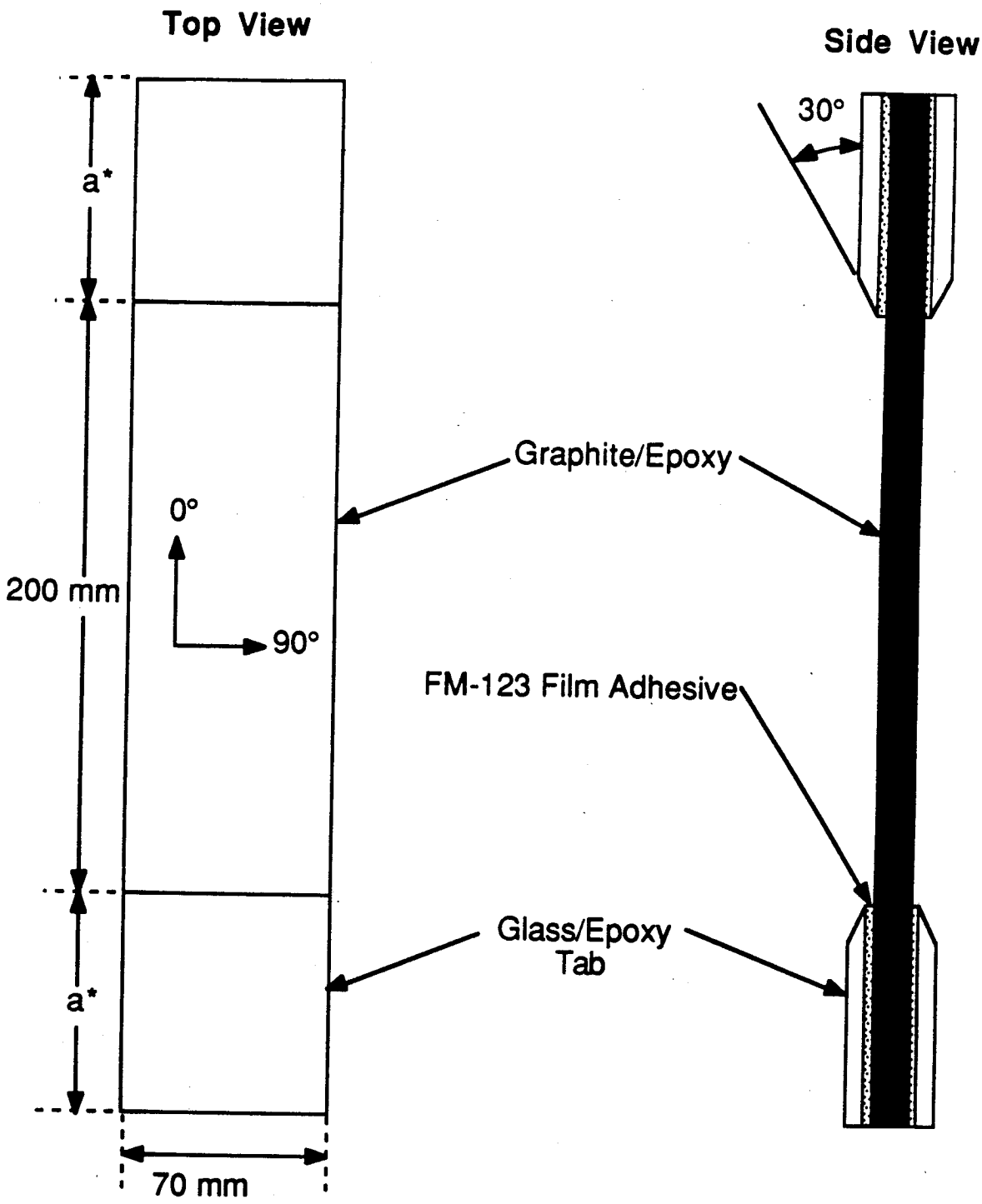

* for $[\pm 45/90]_s$ and $[\pm 45/0]_s$ coupons, a = 75 mm; for $[90/0/\pm 45]_s$ coupons, a = 50 mm

Figure 1 Tensile coupon configuration.

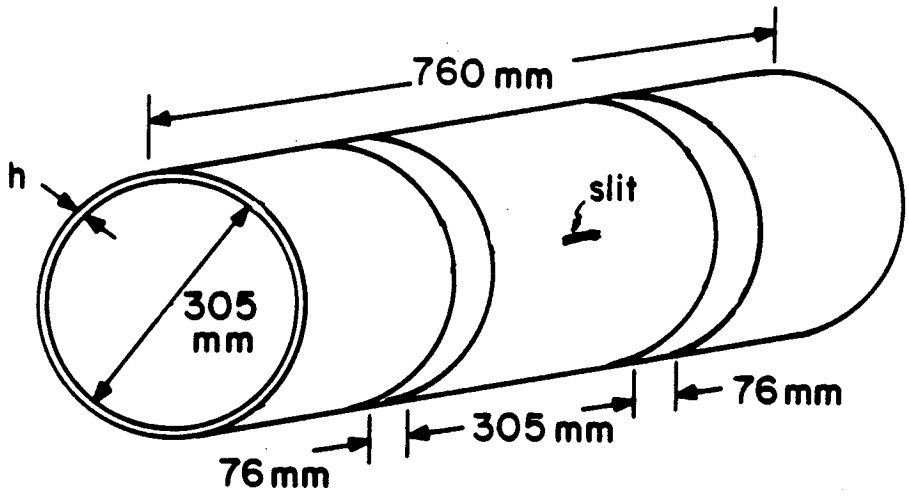

Figure 2 Cylinder specimen configuration.

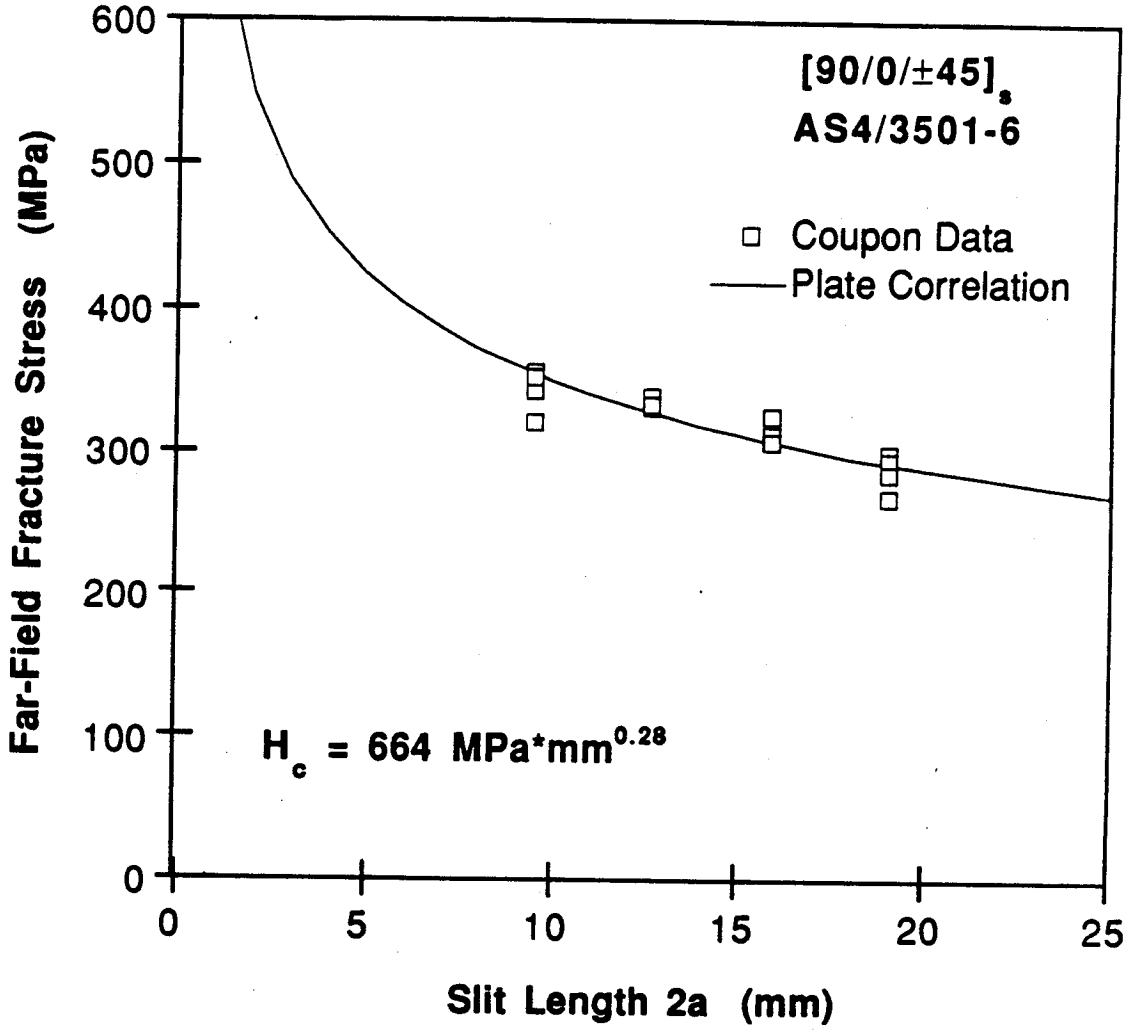

Figure 3 Notched $[90/0/\pm45]_s$ coupon fracture stresses and correlation.

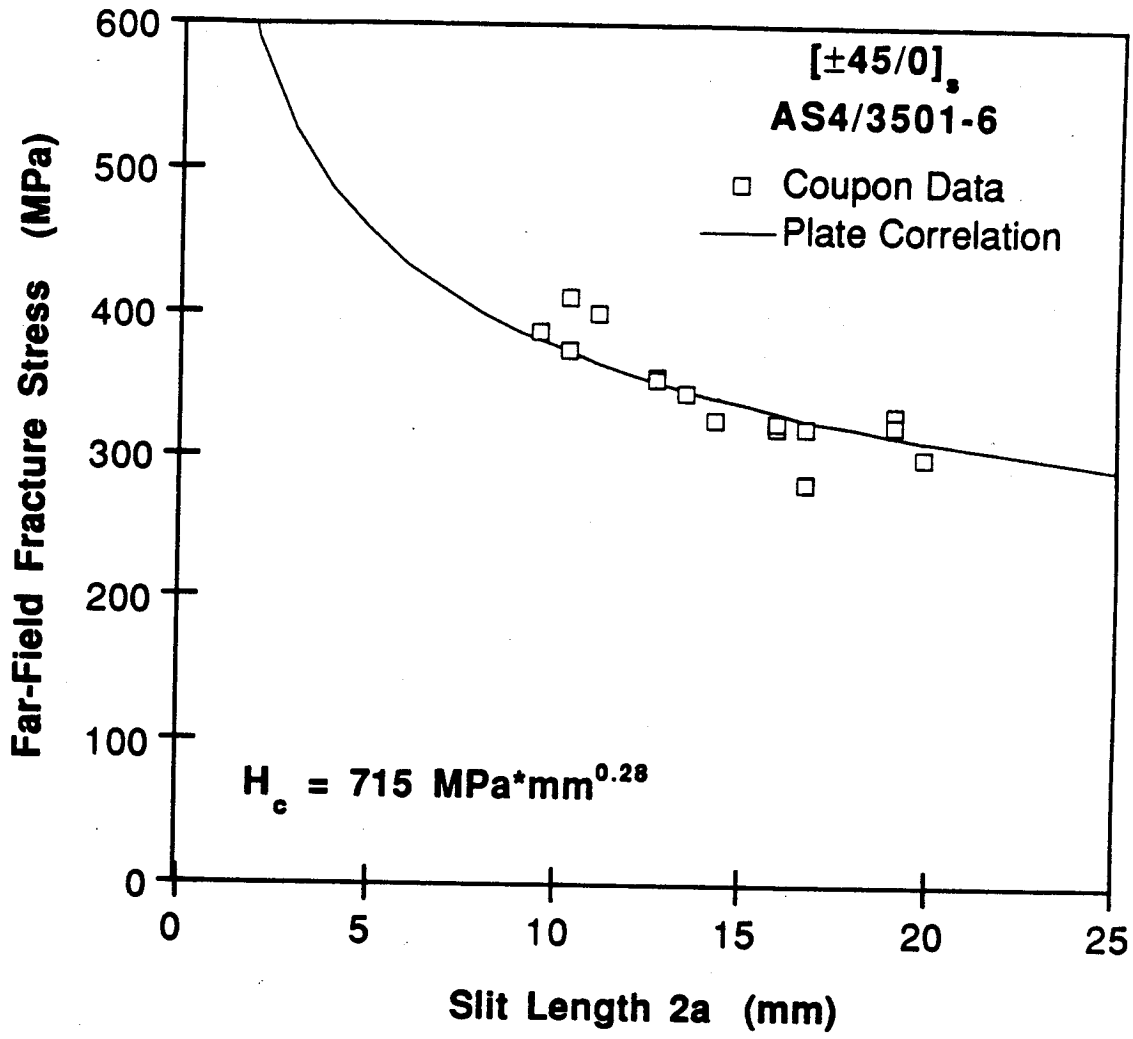

Figure 4 Notched $[\pm 45/0]_s$ coupon fracture stresses and correlation.

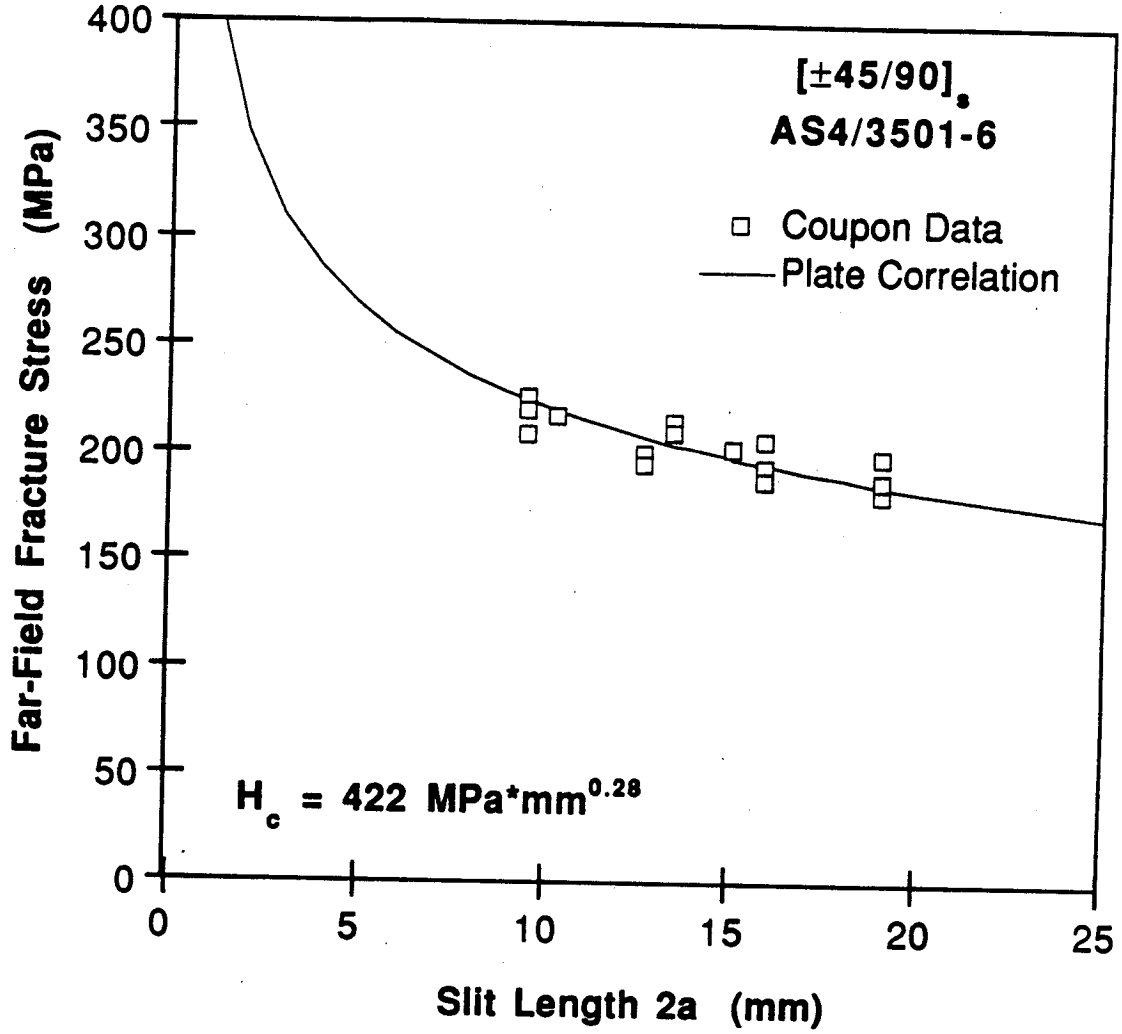

Figure 5 Notched $[\pm 45/90]_s$ coupon fracture stresses and correlation.

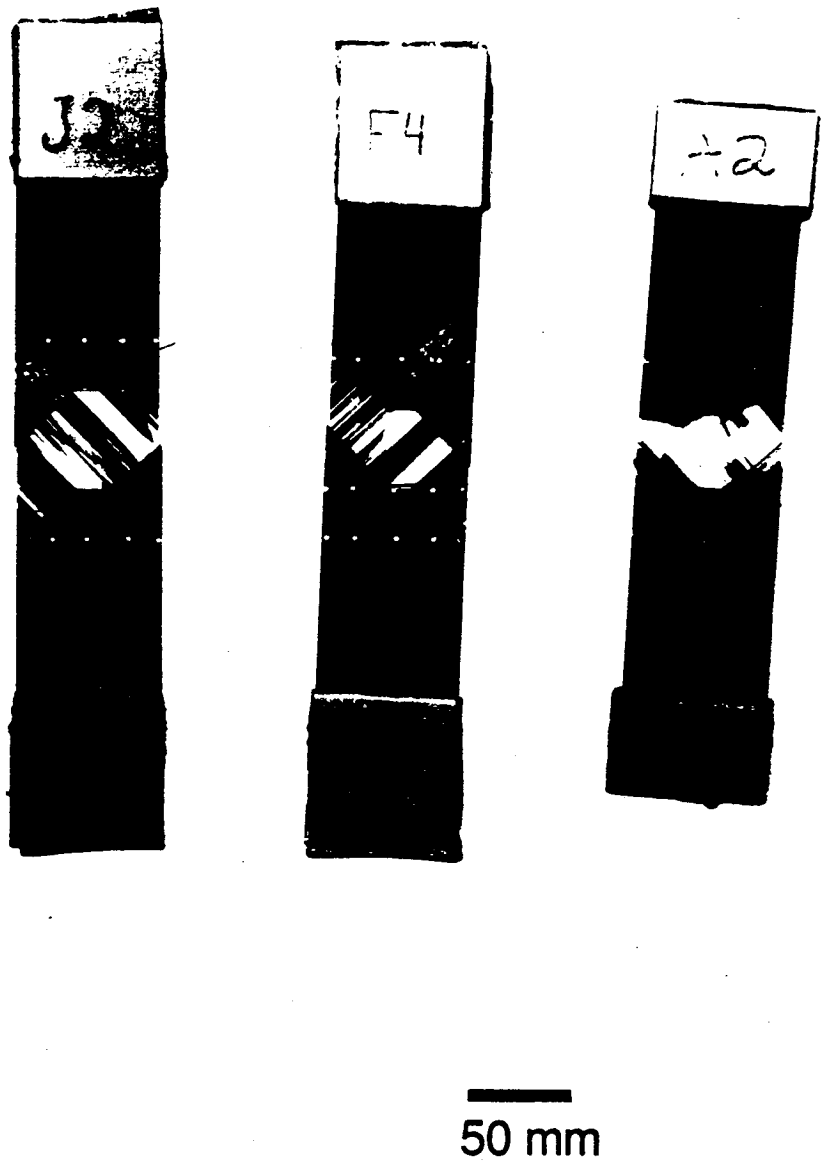

Figure 6 Photographs of fractured *(left)* $[90/0/\pm45]_s$, *(center)* $[\pm45/0]_s$, and *(right)* $[\pm45/90]_s$ coupons with 12.7 mm slit.

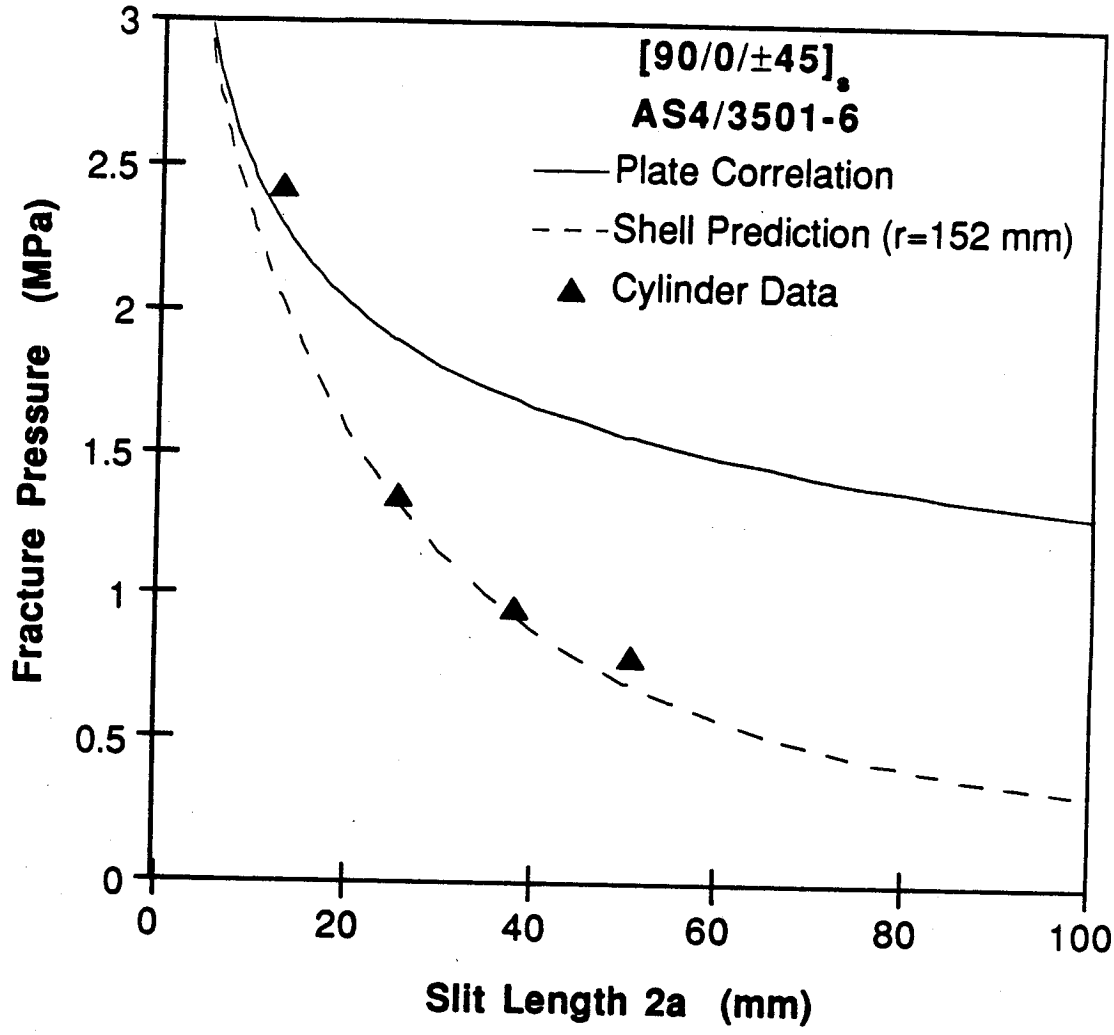

Figure 7 $[90/0/\pm45]_s$ cylinder fracture pressures and predictions.

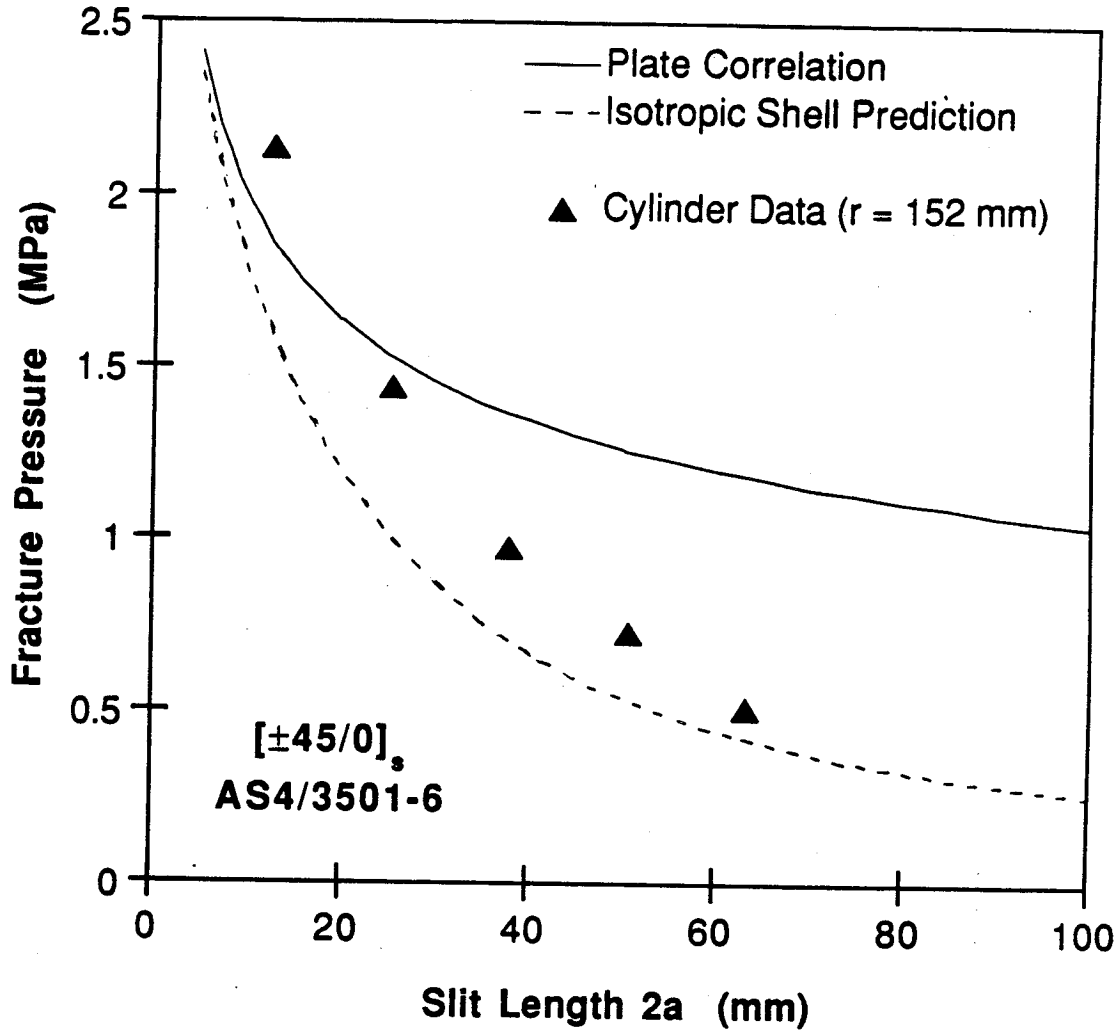

Figure 8 $[\pm 45/0]_s$ cylinder fracture pressures and predictions.

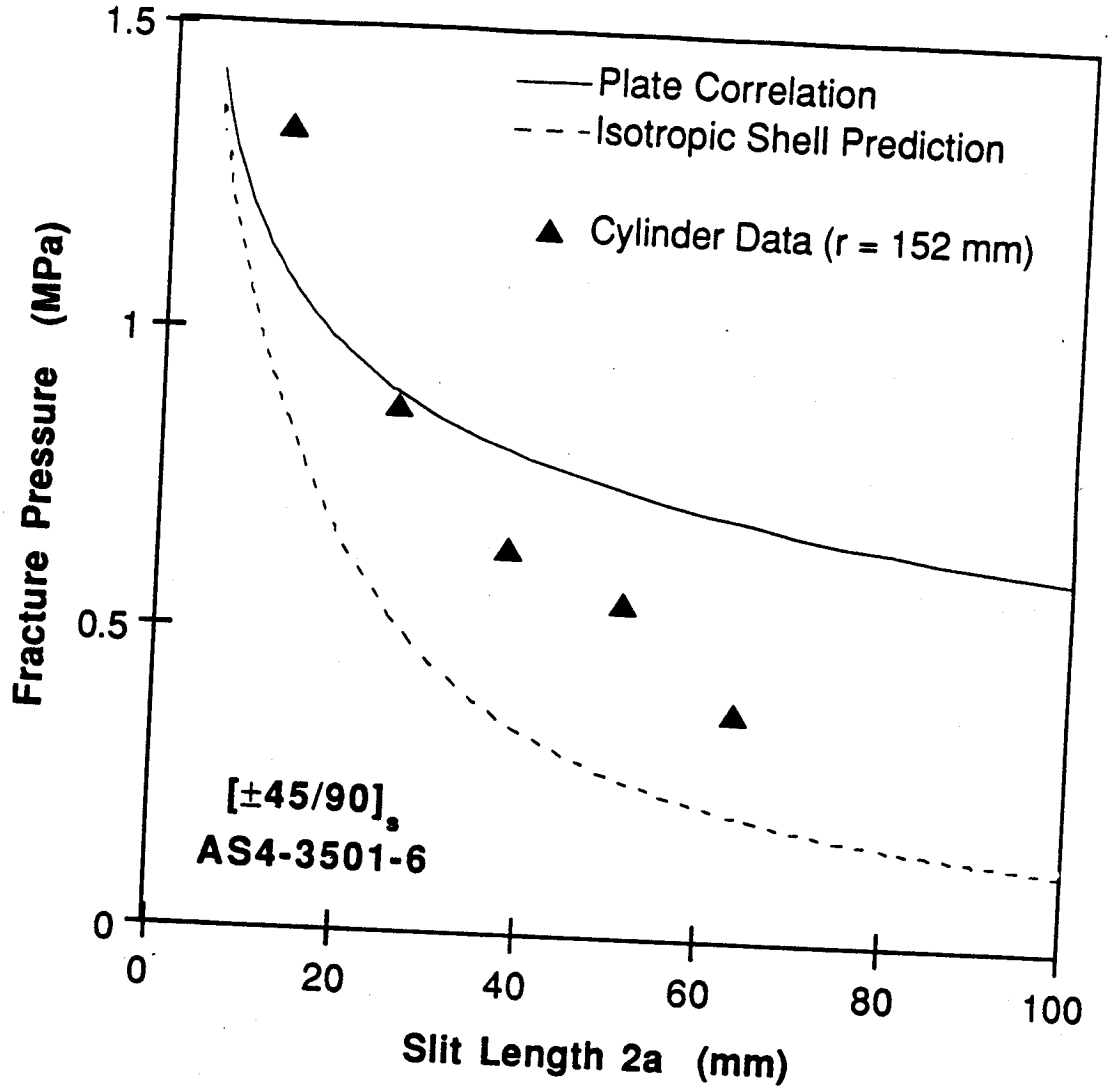

Figure 9 $[\pm 45/90]_s$ cylinder fracture pressures and predictions.

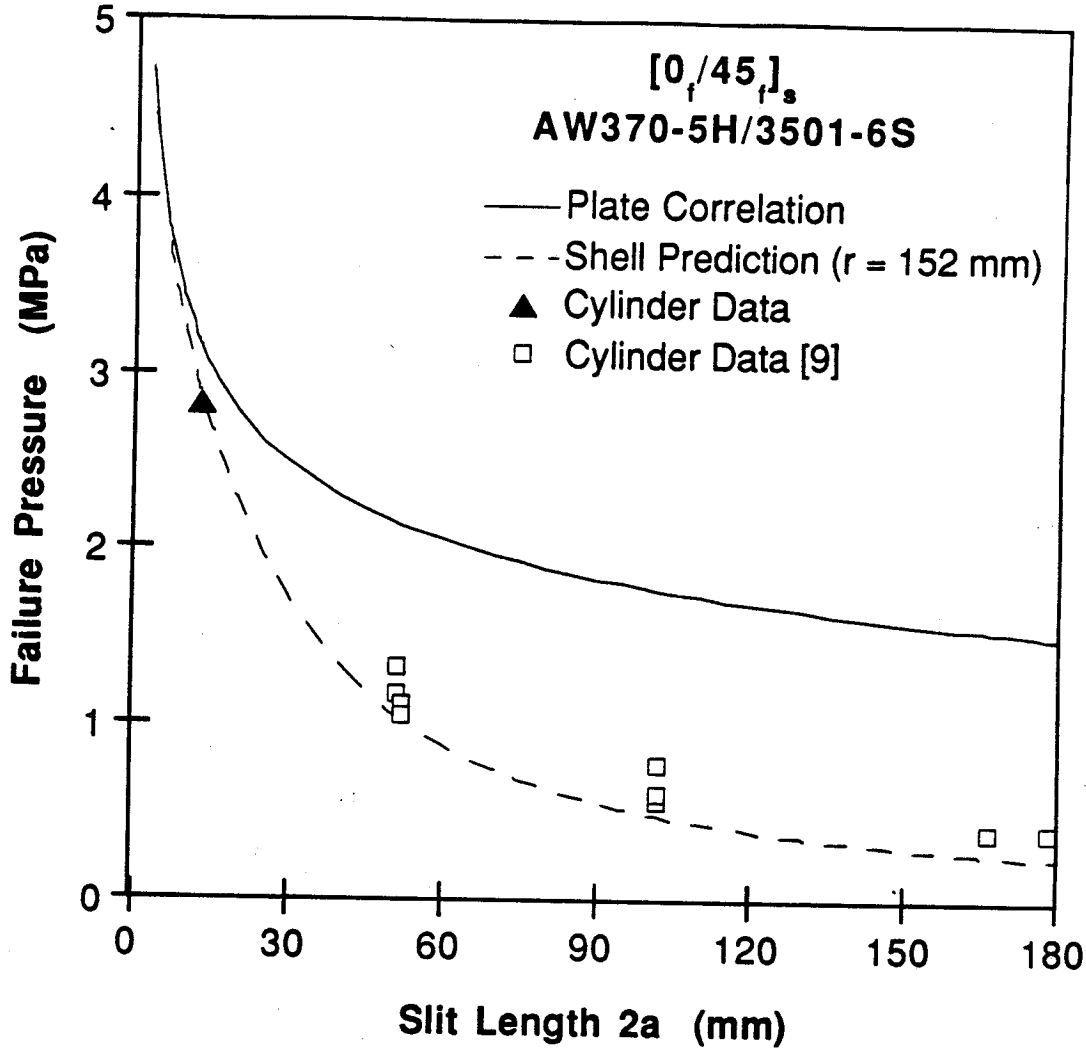

Figure 10 $[0_f/45_f]_s$ cylinder fracture pressures and predictions.

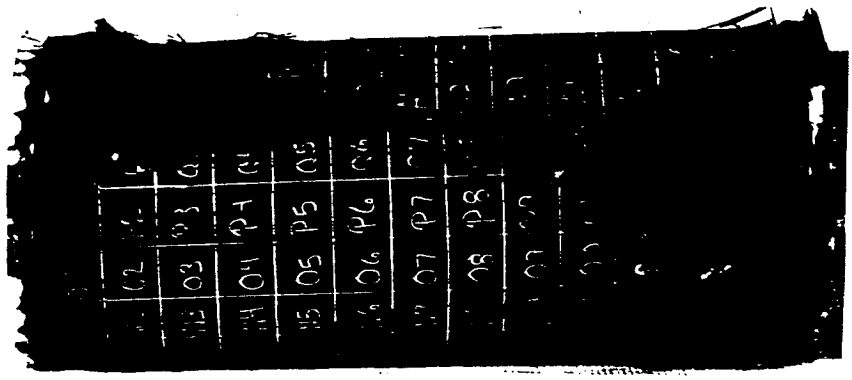

100 mm

Figure 11 Photograph of failed $[90/0/\pm45]_s$ cylinder with 50.8 mm slit and no layers of stiffeners.

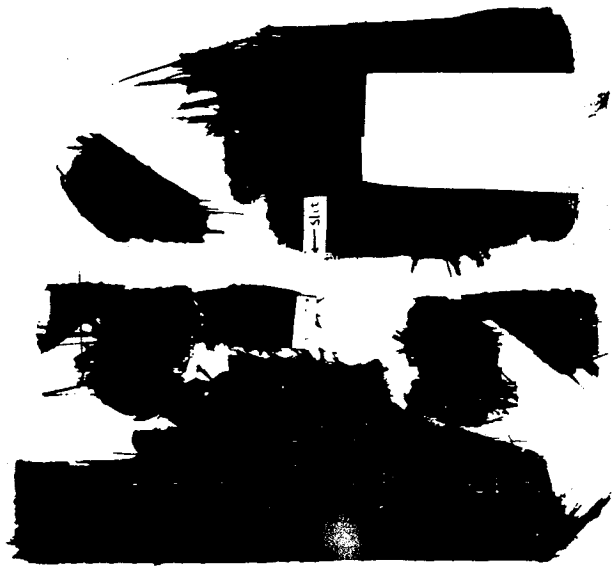

Figure 12 Schematic of failed $[90/0/\pm45]_s$ cylinder with 12.7 mm slit and no layers of stiffeners.

100 mm

Figure 13 Photograph of failed $[\pm 45/0]_s$ cylinder with 63.5 mm slit and two layers of stiffeners.

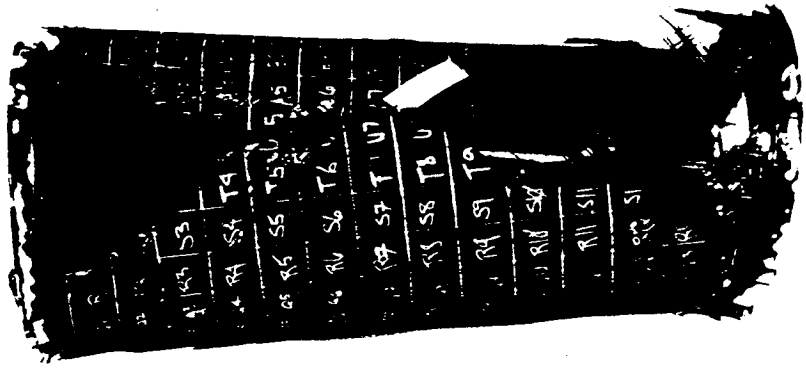

100 mm

Figure 14 Photograph of failed $[\pm 45/90]_s$ cylinder with 38.1 mm slit and no layers of stiffeners.

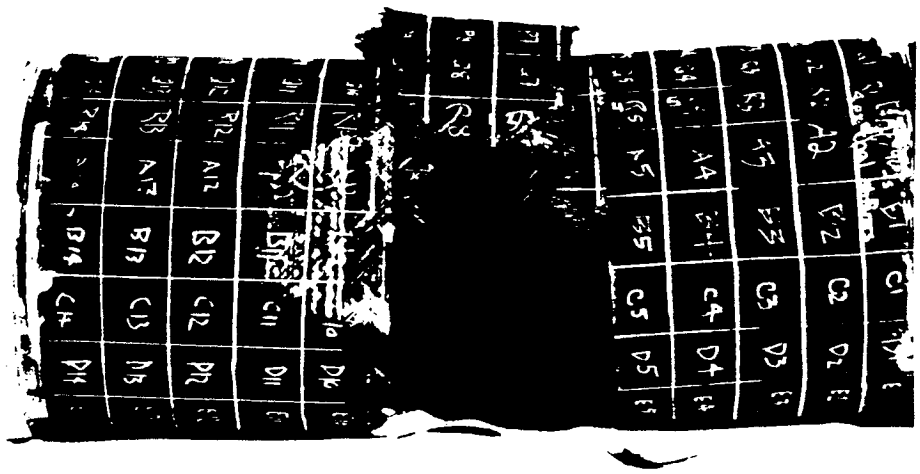

100 mm

Figure 15 Photograph of failed $[\pm 45/0]_s$ cylinder with 38.1 mm slit and four layers of stiffeners, showing bifuraction of fracture path.